Evaluating Spatial Understanding of Large Language Models

Anonymous authors
Paper under double-blind review

Abstract

Large language models (LLMs) show remarkable capabilities across a variety of tasks. Despite the models only seeing text in training, several recent studies suggest that LLM representations implicitly capture aspects of the underlying grounded concepts. Here, we explore LLM representations of a particularly salient kind of grounded knowledge — spatial relationships. We design natural-language navigation tasks and evaluate the ability of LLMs, in particular GPT-3.5-turbo, GPT-4, and Llama2 series models, to represent and reason about spatial structures. These tasks reveal substantial variability in LLM performance across different spatial structures, including square, hexagonal, and triangular grids, rings, and trees. We also discover that, similar to humans, LLMs utilize object names as landmarks for maintaining spatial maps. Finally, in extensive error analysis, we find that LLMs' mistakes reflect both spatial and non-spatial factors. These findings suggest that LLMs appear to capture certain aspects of spatial structure implicitly, but room for improvement remains.

1 Introduction

Large language models (LLMs) show remarkable capabilities in language, and also hints of implicitly learning about the grounded concepts beyond language. For example, language models can develop semantically-organized internal representations for basic concepts like color and direction Abdou et al. (2021); Patel & Pavlick (2022) — which can allow grounding the models with only a few examples. Furthermore Li et al. (2021) demonstrate that internal representations of language models can dynamically track the states of entities and their relations during discourse. Human language use manifests the semantics of the world from which it originates, and thereby might allow LLMs to implicitly learn something about the entities and processes that exist in the physical world.

Natural intelligences extract and use such knowledge of the physical world – often referred to as world models. A particularly salient example is the ability of humans and animals to create and manipulate mental maps, which serves as a fundamental prerequisite for flexibly navigating and interacting with their environments. Cognitive maps Tolman (1948) were suggested as a metaphor for mental representations that enable adaptable behavior such as planning routes or finding shortcuts. The quest to uncover how the brain represents such maps has led to significant discoveries about the neural mechanisms underlying such maps, such as place cells O'Keefe & Dostrovsky (1971), grid cells Hafting et al. (2005), and boundary cells Lever et al. (2009). While navigation generally involves active, grounded experience, some studies suggest that humans use similar representational structures for abstract knowledge as well (e.g. Whittington et al., 2020). Furthermore, cognitive and neural evidence suggests that humans and animals can learn spatial structure solely from sequences of observations Whittington et al. (2022); Garvert et al. (2017). This raises an intriguing possibility – that LLMs might also be capable of inferring sophisticated spatial relations from their sequential, text-based inputs.

In this paper, we examine the spatial understanding capabilities of LLMs – in particular OpenAI's GPT-3.5-turbo, GPT-4 models as well as Llama2-7B, Llama2-13B, Llama2-70B, CodeLlama-34B models Touvron et al. (2023). We designed a broad set of navigation tasks rendered in natural language such that successfully solving these tasks requires accurately representing the underlying spatial relations. These relations include grids with square, hexagonal, and triangular topologies, in addition to rings and trees. Our study reveals

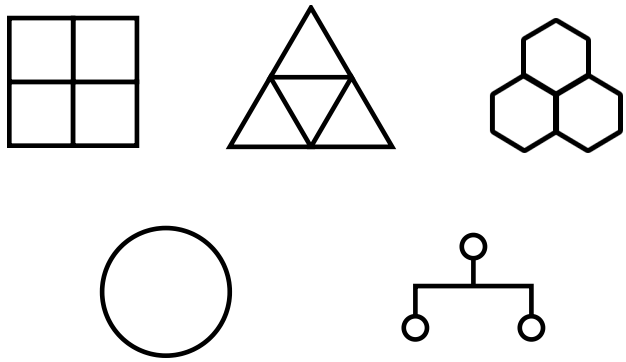

Figure 1: The spatial structures we examine for the underlying maps include squares, triangles, hexagons and rings. Additionally, we analyze a tree structure to explore its relational nature.

that LLMs exhibit varying performance when the underlying spatial structures differ (§3.1). We also observe that presenting the global map upfront actually makes the task more challenging compared to providing local navigational instructions only (§3.2). Moreover, we investigate the effect of the spatial patterns (e.g., random order, row-major) by which global map is expressed on the performance of LLMs (§3.3). We also provide evidence that LLMs spontaneously utilize object information as landmarks for constructing spatial maps (§3.5), much like humans and animals. Finally, detailed error analyses (§4) confirm that in spatial structures that LLMs perform well, their mistakes manifest the underlying spatial topology, as well as non-spatial factors. These error distributions suggest that GPT-4, which often substantially outperforms GPT-3.5, seems to implicitly grasp certain elements of spatial structure, but there is still room for improvement.

We believe gaining insights into the spatial comprehension abilities of LLMs is valuable in enhancing our understanding of how these models acquire and grasp grounded concepts.

2 Spatial Understanding Task

How can we evaluate the text-only models' understanding of spatial information? With human participants, we could have them explore the environment and then ask them to draw a map. However, for text-in, text-out models like LLMs, formalizing the task of spatial reasoning is difficult because these models lack the capability to directly interact with the physical world or visually draw the entire map. However, some studies in human cognition Garvert et al. (2017) have presented participants with sequential data that is sampled from an underlying spatial structure. These studies suggest that humans implicitly acquire knowledge and learn representations that mirror the spatial structure that is latent in the data. This motivates the hypothesis that presenting sequential transitions might be enough for LLMs to achieve spatial understanding.

For example, if a model comprehends a square map's structure, it should be able to answer the following question: "You start at a spot where you find an apple. You move up and find a banana. Then you move right and find an orange. Next, you move down and find a grape. Now, you move left. What do you find?" Answering this question correctly demonstrates an understanding of loop closure, which is a fundamental aspect of this spatial structure. That is, if we have a square grid and an initial location, we can allow the model to take a random walk until it reaches a location it has already visited before. At each newly visited location, we inform the model about the objects it perceives, and then we ask the model which object it would have seen just before reaching the already visited location. By generating such questions synthetically, we can systematically evaluate the spatial understanding of LLMs. For each question, we randomly select the object names from the ImageNet-1k labels to fill every location of the spatial grid to create the underlying map.

Question: "You have been given a 2 by 2 square grid. Starting from a vertex, you will move along the edges of the grid. Initially, you are positioned at the bottom left corner of the grid, where you find a box turtle. You move right by one step, where you find a table lamp. You move up by one step, where you find an American black bear. You move left by one step, where you find a hand plane. You move down by one step. What will you find?"
Answer: "box turtle"

(a) Square

Question: "You have been given an equilateral triangular tile map consisting of 2 rows, where the first row has one tile and the second row has three tiles. Starting from a vertex, you will move along the edges of these tiles. Initially, you are positioned at the bottom left corner of the map, where you find a box turtle. You move right by one step, where you find a hand plane. You move up-right by one step, where you find a guacamole. You move down-right by one step, where you find a table lamp. You move left by one step. What will you find?"
Answer: "hand plane"

(b) Triangle

Question: "You have been given a pointy-topped regular hexagonal tile map consisting of 1 tile. Starting from a vertex, you will move along the edges of the tile. Initially, you are positioned at the top corner of the map, where you find an ice pop. You move down-right by one step, where you find a Boxer. You move down by one step, where you find a poke bonnet. You move down-left by one step, where you find a combination lock. You move up-left by one step, where you find a spotlight. You move up by one step, where you find a gibbon. You move up-right by one step. What will you find?"
Answer: "ice pop"

(c) Hexagon

Question: "You have been given a circular grid consisting of 4 connected dots. Starting from a vertex, you will move along the edges of the circular grid. Initially, you are positioned on the dot that's located at the top of the grid, where you find a palace. You move around the ring by 1 step in a clockwise direction, where you find a gong. You move around the ring by 2 steps in a clockwise direction, where you find a shopping basket. You move around the ring by 2 steps in a clockwise direction. What will you find?"
Answer: "gong"

(d) Ring

Figure 2: Example question and its answer for square, triangle, hexagon and ring structure.

2.1 Models and evaluation metrics

We test GPT-3.5 (gpt-3.5-turbo-0301), GPT-4 (gpt-4-0314), Llama2-7B, Llama2-13B, Llama2-70B, and CodeLlama-34B. All Llama models are Llama-Chat models and the CodeLlama model is the Instruct variant. The context window sizes for these models are 4,096 tokens except for GPT-4, which has 8,192 tokens. We focus on zero-shot experiments, where we used the following system prompt: "You are given a task to solve. Make sure to output an answer after "Answer:" without any explanation."

To ensure consistent evaluation, we utilize the following protocol: We first check if the generated text contains the keyword "Answer:". If present, we consider the subsequent text as the model's prediction. In situations where there are multiple ground-truth answers, we store the answers as a set using "," as the separator. We consider the prediction correct only when the generated set of answers matched the ground-truth set exactly.

3 Results

3.1 Do different spatial structures affect model performance?

In Section 2, we provide an example that utilizes a square grid to assess the understanding of spatial structures in LLMs. In the example, we exploit the concept of loop closure within the square grid for this purpose. Since loop closure also exists in other spatial structures like rings, hexagons, and triangles, we can evaluate how the model's performance on spatial understanding is influenced by different spatial structures. As for our choice of spatial structures, we begin with squares because they are the most straightforward 2D structure. We have also included triangles and hexagons to explore how well LLMs comprehend less common 2D structures.

To ensure a fair comparison across these structures, we generate synthetic text prompts similar to the square grid scenario and keep the number of steps to be 8. We use a 3 by 3 square grid, size 2 hexagonal grid, size 3 triangular grid, and size 12 ring grid as the underlying maps. Example prompts are shown in Figure 2.

The results are shown in Figure 3. When comparing GPT-3.5-turbo and GPT-4, we find that GPT-3.5-turbo performs poorly across all spatial structures, while GPT-4 shows higher variation in performance. GPT-4 excels on the Square structure, ranks second best on the Ring and Triangle structures, and performs the worst on the Hexagon structure. Llama2-70B and CodeLlama-34B, while generally performing worse than GPT-4, exhibit a similar pattern of performance to GPT-4. We omit Llama2-7B and 13B from our discussion because they achieve zero (or very close to zero) accuracy across all structures. This indicates that tackling zero-shot spatial reasoning tasks may necessitate larger models.

Of particular interest is LLM's proficiency in handling square structures compared to other types. Is this phenomenon explainable by low-level graph features such as the number of edges and vertices? To see this,

we run a logistic regression analysis to examine what influences the binary prediction outcomes. Specifically, using the square type as the reference level for graph types, we analyze the prediction outcomes via the following model: Prediction correctness $\sim$ intercept + $\mathbf{1}$(graph type == hexagon) + $\mathbf{1}$(graph type == triangle) + $\mathbf{1}$(graph type == ring)+ number of edges + number of steps. We only pick the number of edges as our low-level graph feature because the correlation between the number of edges and the number of vertices is very high (correlation coefficient was 0.998). We collect 6,100 prediction results of GPT-4 varying the structure type, the number of steps, and the number of edges (i.e. hexagon: 1400 samples, ring: 1500 samples, square: 1800 samples, and triangle: 1400 samples). The summarized results are presented in Table 1. We observe that the accuracy of predictions is not significantly influenced by the lower-level graph feature (i.e. the number of edges). However, it does depend on higher-level graph structure. Furthermore, we note that the accuracy is heavily influenced by the number of exploration steps (p value $<$ 2e-16). This finding aligns with our intuition, as longer navigation poses greater challenges in tracking objects in a spatial map.

The relative ease of the square grid in comparison to other grid types could be attributed to factors such as the prevalence of tabular data and city grid navigation within the model's training data. In addition, coding problems related to maze exploration often involve navigating a two-dimensional square grid, while triangular and hexagonal grids are less commonly encountered. Thus, it is conceivable that such exposure during pre-training makes GPT-4 possess an enhanced understanding of 2D square grids. Analogously, for humans, individuals who grow up in cities with a more grid-like structure may exhibit greater difficulty in navigating through less organized environments, such as older European cities, and vice versa Coutrot et al. (2022). Additionally, we perform an experiment using the rhombus grid, which was achieved by rotating the square grid 90 degrees. Under the same experimental condition, we find that GPT-4 maintains an accuracy of 0.66, which is slightly lower than the original square-grid accuracy of 0.71 but still significantly higher than other structures. This outcome provides further confirmation that the specific grid structure with two axes contributes to its strong performance.

	Estimate	Std. Error	z value	Pr(>|z|)
(Intercept)	3.448	0.142	24.273	<2e-16 (***)
type.hexagon	-2.327	0.091	-25.595	<2e-16 (***)
type.triangle	-1.820	0.082	-22.199	<2e-16 (***)
type.ring	-2.117	0.103	-20.616	<2e-16 (***)
number of edges	-0.002	0.002	-1.062	0.288
number of steps	-0.345	0.018	-18.924	<2e-16 (***)

Table 1: Logistic regression results. We see that the number of edges (an example of lower-level features) is not a significant predictor variable for prediction correctness (p value = 0.288). However, the higher-level graph structure (e.g. square or hexagon) is a significant predictor of correctness (all p values $<$ 2e-16).

3.2 Is building a local map more difficult than building a full map and retrieving a path?

In the previous section, LLMs were tasked with constructing a local map gradually as they received new information, one step at a time, which we refer to as the "local" setting. Alternatively, we can provide LLMs with the complete map from the start and instruct them to begin exploration from a randomly selected initial location for a specific number of steps, which we refer to as the "global" setting. On one hand, local exploration may be deemed easier as it requires retaining less information. On the other hand, presenting the global map upfront could potentially aid in more accurate map navigation. To address this question, we compare the local and global settings in our spatial understanding task. For this comparison, we use Square and Ring structures since there are widely accepted methods of specifying global coordinates, making it easier to specify paths from a randomly selected initial position. In particular, we provide the global map information in the following manner: For the square structure, we list the object names row by row. As for the ring structure, we list the object names starting from the top and proceed clockwise. We then have the model follow a fixed number of navigation instructions, just like the local setting. An example prompt is given in Appendix. The results in Figure 4 show that the global setting is slightly harder than

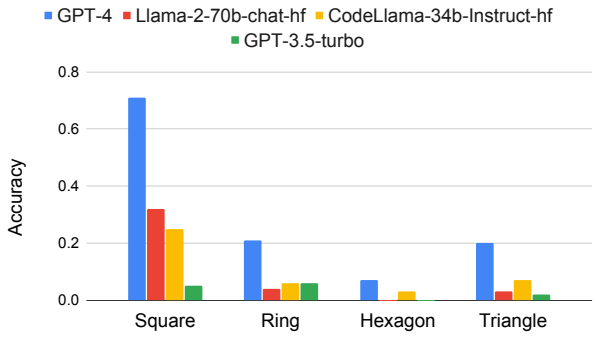

Figure 3: We compare the accuracy of the models across the different spatial structures. The random guessing accuracy is 1/8 since the predictions from random guessing are uniformly selected from the nodes encountered by the models, which corresponds to the local path with 8 navigation steps. GPT-4 have higher prediction accuracy than random guessing in square, ring and triangle structures, but worse in hexagon. ChatGPT exhibits lower prediction accuracy than random guessing across all of these structures. Llama2-70B and CodeLlama-34B shows a similar pattern to GPT-4.

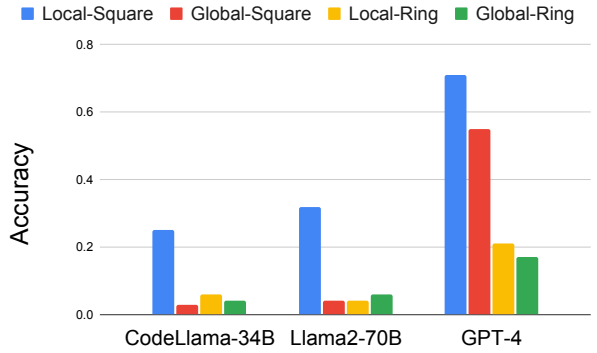

Figure 4: Performance is evaluated on GPT-4, Llama2-70B, and CodeLlama-34B. For both square and ring structures, we observe that the prediction accuracy of GPT-4 using the local map is higher compared to the global map. Llama2-70B and CodeLlama-34B show a similar pattern for Square, while the pattern is less clear for Ring.

the local setting for both Square and Ring structures, except when the performance is already low for the ring structure for Llama2 models, which shows a less clear pattern as such.

The results presented in Figure 4 show that, in general, the global setting is more challenging than the local setting for both Square and Ring structures. However, this trend becomes less evident when considering the already low performance of Llama2 models on the Ring structure, leading to a less clear pattern in this case.

3.3 The order of presenting the map impacts spatial understanding

In the previous section, our approach to providing complete map information upfront to the model has involved a specific method. We describe the items in the map row by row, indicating their positions from left to right. For example, in the first row, we have item A, item B, and item C. In the second row, we have item D, item E, and item F from left to right, and so on. However, there exist multiple ways to convey the same information. Here, we explore different approaches to feeding data into the model. In addition to the aforementioned method, we examine two alternative techniques: random and snake order. The random approach involves placing items in the map at random positions using the global coordinate system. On the other hand, the snake order method follows a specific pattern. In the first row, items are fed from left

to right as before. However, when transitioning to the second row, we introduce the instruction "you move down by one step" to indicate the change in row. In the second row, items are then fed from right to left. By investigating these alternative data feeding methods, we aim to understand their implications and assess their impact on the model's performance.

The results are shown in Table 2. Although the GPT-4's accuracy degrades for Random and Snake, it is noteworthy that Random is better than Snake. We note that we omit the results for Llama-2 models because even Llama2-70B's performance was already very low (e.g. row-by-row's accuracy is 0.04 for Llama2-70B whereas GPT-4 achieves 0.55.)

	Row-by-row	Random	Snake	Snake+Coord
GPT-4 Acc	0.55	0.485	0.4	0.56

Table 2: The order of presenting the map impacts spatial understanding accuracy. Snake+Coord refers to the setting where we append the global coordinates of the location after each step.

What could potentially explain these phenomena? It is reasonable to speculate that different methods of inputting data could influence how LLMs internally represent spatial relations. For instance, when utilizing the row-by-row approach, the LLM can register these items in a key-value dictionary, where the row id serves as the key and a list of objects represents the corresponding value. The 'random' approach also enables the LLM to store a key-value dictionary where the key denotes the location address and the value denotes a single item, which can be leveraged for navigation purposes later on. On the other hand, the 'snake' order approach necessitates the LLM to simultaneously handle the storage of object item information and spatial relational understanding. This added complexity potentially complicates the task.

To investigate whether or not such a key-value data structure plays a role, we perform an additional experiment where we add the global coordinate information to the snake order approach. We see that this approach indeed increases the accuracy from 0.4 to 0.56, corroborating our hypothesis.

3.4 Relational structure: Tree

In addition to spatial structures, relational structures can also be represented using connected graphs. In this section, we examine a tree structure. Unlike spatial structures, the hierarchical structure of a tree is more naturally presented in a global setting, where all objects are provided at the beginning, and relational questions can be asked subsequently.

To ensure comparability with the square and ring structures, we set the number of nodes in each tree to be 9. For comparison, we also included a 3 by 3 square grid and a 9-node ring in this experiment. The exploration steps are set to 4 for all structures. For the tree structure, we utilize the same ImageNet object labels, but focus on relational questions that involve 4 steps, such as "What is the cousin of A?", "What is the great-great-grandparent of A?", and "What is/are the great-great-grandchild/children of A?". An illustrative example question and its corresponding answer can be found in Figure 5.

The results are depicted in Figure 6. We observe that for GPT-4, while the tree structure performs worse than the square structure, it outperforms the ring structure. On the other hand, for GPT-3.5-turbo, the tree structure exhibits better performance compared to the square structure. We observe that just like GPT-3.5-turbo, Tree performs better than Square for all Llama-2 models. The only exception is GPT-4; this further demonstrates that GPT-4's exception ability to comprehend the square structure. We also note that Ring is harder than Square for all Llama models and GPT-4. Further investigation into how relational structure, spatial structure, and model size impact performance would be an intriguing topic for future research.

3.5 Grid size inference from sequences of navigational instructions

In the preceding sections, we examined the capability of LLMs to understand the spatial and relational structure of a map. In this section, our focus shifts to investigating whether LLMs can infer the global size of a map based solely on a sequence of local navigational actions. Specifically, we provide navigational

Question: "You have been given a tree structure with 9 nodes. The root node is a great white shark. The great white shark has 2 children: a garter snake and a Gila monster. The garter snake has 2 children: a jigsaw puzzle and a moped. The jigsaw puzzle has a child: a Tibetan Terrier. The Tibetan Terrier has no children. The moped has a child: an umbrella. The umbrella has no children. The Gila monster has 2 children: a Christmas stocking and a horse-drawn vehicle. The Christmas stocking has no children. The horse-drawn vehicle has no children. What is the cousin of the moped? "
Answer: "Christmas stocking, horse-drawn vehicle"

Figure 5: Example prompt for tree structure.

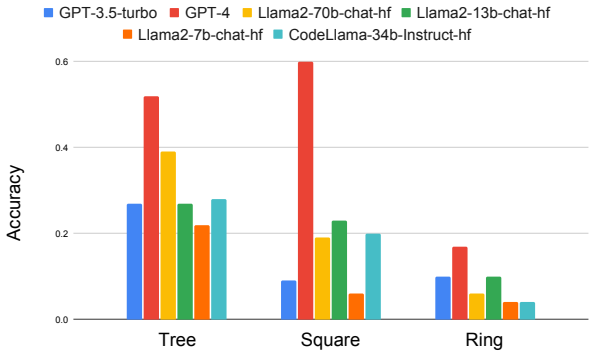

Figure 6: We evaluate the prediction accuracy of the models on a 9-node tree, a 3 by 3 square, and a 9-node ring structure with 4 exploration steps in the global setting. Comparing the performance of GPT-4 and random guessing, GPT-4 outperforms random guessing with higher prediction accuracy, with the order of accuracy being square > tree > ring. GPT-3.5-turbo also performs better than random guessing on the tree structure, but worse on the square and ring structures, with the order of accuracy being tree > ring > square. Just like GPT-3.5-turbo, Tree performs better than Square for all Llama-2 models.

instructions that guide the exploration of all locations within a rectangle. As before, we also provide what item the agent finds at each step. Then we ask LLMs about the height and width of the rectangle. This task necessitates LLMs to maintain the entire path in order to accurately deduce the overall dimensions of the rectangle.

Table 3 illustrates the accuracy comparison of GPT-4 for different size configurations of the same area (e.g., 2 by 6, 3 by 4 for an area of 12). We prepare 100 samples for each area. We observe a general trend where accuracy decreases as the length of the sides increases and as the area size of the rectangular grid increases. We omit the results for GPT-3.5-turbo, Llama-2-70B and CodeLlama-34B because these models were not able to infer the size of rectangle.

	3x4 or 4x3	2x6 or 6x2	4x6 or 6x4	3x8 or 8x3	2x12 or 12x2
GPT-4 Acc	0.63	0.22	0.18	0.04	0.01

Table 3: Grid size inference performance of GPT-4.

Additionally, we evaluate the same setup but exclude object item information during navigation. In this case, GPT-4 relies solely on directional information (e.g., "you go up by one step, then you go down by one step, etc."). To our surprise, we consistently find that the setting with directional information alone performs worse than the setting that incorporates both directional and item information, as shown in Figure 7. This might suggest that object items play a role in serving as anchors for improved spatial understanding.

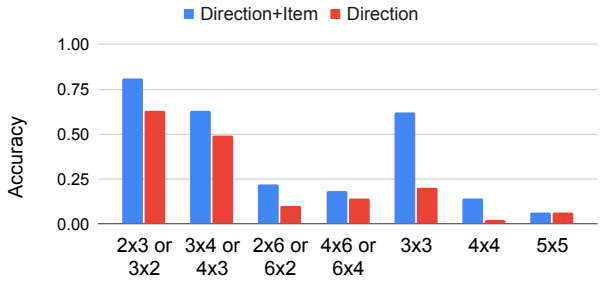

Figure 7: Using only directional information yields poorer performance compared to the approach that combines both directional and object item information at each step.

4 Error analysis

In this section, we perform a detailed analysis of the errors produced by GPT-4, to assess whether it is modelling the correct topology. In our error analysis, we focus on GPT-4 because of its relatively strong performance, which reveals intriguing error patterns.

To study the extent to which LLM understands the topology of a given spatial structure, we examine what types of mistakes it makes. In our spatial understanding task, when LLM makes a mistake, in the overwhelming majority of cases, it provides the name of an object at a different location (rather than naming an object that did not appear at all in the prompt). Therefore, we can measure the distance between the correct location and the location of the predicted object with respect to the underlying topology. If the LLM represents the spatial structure of the map, the distribution of these distances will tend to cluster at small values, which we call spatial-topology bias. That is, if the LLM represents spatial structure, we should expect more mistakes for objects topologically close to the correct location, and fewer mistakes for objects farther away. A natural choice for measuring distances in grids is the shortest distance between two vertices in the grid.

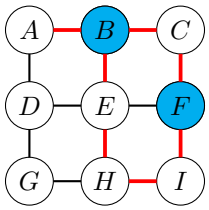

Figure 8: An example of two distance metrics in 3×3 square grid in the local setting. If the path in the local setting starts at node A and follows through B, C, F, I, H, E, and finally ends at B, and if the LLM predicts F instead of B, then the temporal distance between B and F is 4, while the spatial distance is 2.

LLMs may also show non-topological biases in their predictions, an instance of which is the temporal bias – an inclination to predict objects that are observed in the textual vicinity of the ground truth item in the given prompt. To investigate the presence of this bias, we measure the temporal distance as the number of objects between the first occurrence of the ground truth in the prompt and the predicted item (including the predicted item). An illustrative example of the temporal and spatial distances in the local setting is shown in Figure 8.

In the following, we examine the error distributions of GPT-4 in square, triangular, and hexagonal grids. For each experiment, we collect 1000 predictions from GPT-4, and analyze them along with their corresponding prompts and ground-truth correct answers. Out of the 1000 prompts, we only consider the subset of predictions in which the model was wrong. We compare GPT-4's errors with the random distributions of spatial and temporal distances with respect to a uniform baseline. To do this, we randomly pick one of the prompts the model is tested with. Next, we record the location of the ground truth object based on the prompt. Then, for the global setting prompts, we at random select a location from the entire grid; for the

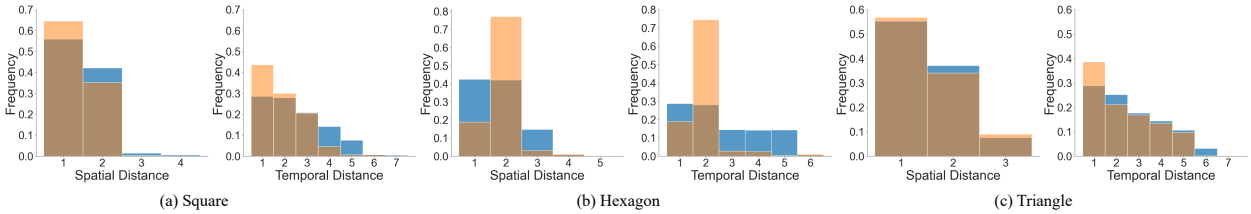

Figure 9: The spatial and temporal distance (SD, TD, respectively) histograms for square, hexagonal, and triangular grids under the local setting. Blue histograms show random baselines. Orange histograms show the observed distribution of errors as the spatial (left) and temporal (right) distances between the ground truth and GPT-4's predicted locations. (a) In grids with square topology, GPT-4 makes more errors both when SD is 1 and TD is 1, compared to the uniform baseline, meaning that both spatial and temporal biases contribute to GPT-4's errors. (b) In grids with hexagonal topology, we do not observe spatial nor temporal bias. (c) The simultaneous lack of spatial bias and the presence of temporal bias indicate that GPT-4 was not able to accurately construct the triangular grid.

local setting prompts, we at random select one of the visited nodes along the path. We then calculate both the spatial or temporal distances between this randomly selected location and the ground truth location. We repeat this procedure for 100,000 times to generate the error distribution for the uniform baselines.

4.1 Comparing error distributions of square, triangular, and hexagonal grids

In our analysis, we used a 3 by 3 square grid, a triangular grid with a size of 3, and a hexagonal grid with a size of 2. We chose these grid configurations to ensure a fair comparison across different grid structures, allowing for prompts conducting 8 navigation steps in each grid. The precise shape of the size-3 triangular grid is shown in Appendix. The size-2 hexagonal grid is shown in Figure 1.

The results for the local setting are shown in Figure 9.

For the square grid, GPT-4 tends to make more errors at spatial distances of 1 relative to random baseline, indicating a spatial-topology bias (Fig. 9a, left). However, temporal distance also shows a stronger peak at the value of 1 (relative to the uniform baseline; Fig. 9a, right) indicating that having two items more closely located in the prompt is also an effective predictor of GPT-4's errors. In Appendix, we also plot the conditional distribution of TD when SD=1 to further validate the temporal bias.

In the case of the hexagonal grid (Fig. 9b), we see a lack of spatial-topology bias, with the distribution of distances peaking at 2 (instead of 1). We also do not see a temporal bias in GPT-4's behavior, again with a distribution peaked at the temporal distance of 2. This indicates the presence of some other source of non-spatial bias besides the temporal bias. Closer inspection revealed that whenever GPT-4 makes an error in hexagonal grids, these errors are often due to the model predicting the very first object on the path, which often ends up having spatial and temporal distances of 2 from the ground truth correct answer.

For the triangular grid (Fig. 9c), the distribution of SD from GPT-4 and random guessing is almost the same, suggesting that there is almost no spatial bias. However, there is a spike when TD = 1. We find that among all the instances where TD equals 1, the proportion of predicting the starting position is 0.416. Hence, it appears that the temporal bias accounts for more than half of the bias observed in the triangular grid. For the starting position bias of the square grid, see Appendix.

In Figure 10, we present analyses for the global structure.[1] When dealing with a square grid, we provide GPT-4 with the complete map upfront by listing each object row by row. For instance, in prompts for the square grid structure in the global setting, such as "In the first row, we have item A, B, and C. In the second row, we have item D, E, and F, ..." the temporal distance between A and D would be 3. If GPT-4 represents the square grid as a one-dimensional array, we expect that the frequency of temporal distance would decrease steadily. However, we observe spikes at 3 and 6 in the temporal distance, which correspond to

[1]We omit the ring structure because each movement can involve many steps around the ring (e.g. "move by 3 steps clockwise"), which effectively introduces edges between all graph nodes, and thus renders analysis based on spatial distance less meaningful.

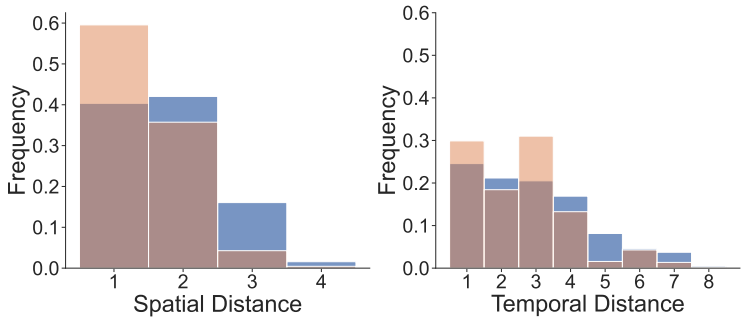

Figure 10: The spatial and temporal error histograms for the 3 by 3 square grid under the global setting. We see a spike when the temporal distance (TD) is 3 and 6, indicating an effect of spatial distance – these two TD values correspond to the spatial distance of 1 and 2.

spatial distances of 1 and 2, respectively. This finding suggests that GPT-4 makes more errors when objects are closer to the ground truth in terms of spatial structure, rather than temporal distance. It supports the notion that GPT-4 actually models some aspect of the two-dimensional structure. Furthermore, we investigate whether there are any discrepancies in error distributions when the distance is calculated using either row-major order or column-major order. Figure 11 demonstrates that there is an almost symmetrical distribution between rows and columns. This provides additional evidence that GPT-4 recovers the structure of the two-dimensional array.

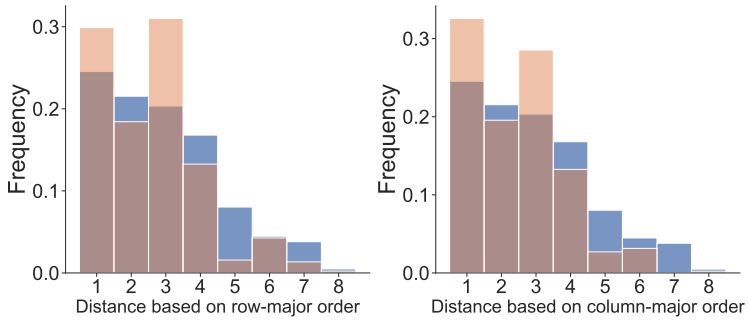

Figure 11: The row-wise and column-wise error histograms for the 3 by 3 square grid with 8 exploration steps under the global setting. We see that both row and column-wise histograms are almost identical, which suggests GPT-4 does not have bias for row or column.

5 Comparison to human baseline

Finally, we have conducted human experiments to assess the average human baseline performance. These experiments focused on local navigation tasks using the structures shown in Figure 3, which include a 3 by 3 square grid, a size 2 hexagonal grid, a size 3 triangular grid, and a size 12 ring grid. For each of these structures, we randomly selected 20 prompts from the previously used dataset, resulting in a total of 80 candidate prompts. Then, for each participant in the experiment, we randomly chose 10 prompts from this pool of candidate prompts. Participants were asked to provide textual answers to these questions. Additionally, we included 4 attention check questions. These questions were intentionally designed to be easy so that we can assess whether participants were providing meaningful answers, and were used as an exclusion criterion in our analysis. These attention check questions were drawn from the set of questions associated with very simple structures, such as a 2 by 2 square grid, a size 1 hexagonal grid, a size 2 triangular grid, and a size 5 ring grid. These attention check questions were distributed randomly throughout the survey.

We established a criterion to measure participants' engagement in the experiment: if a participant made more than one mistake in the attention check problems, we would exclude their response from the analysis.

Specifically, each participant had 30 minutes to solve 14 problems, which consisted of 10 regular problems to evaluate human performance and 4 attention check problems. The participants were not informed whether the given problem was a regular task or an attention check.

In this experiment, we received completed responses from a total of 23 participants. Among them, 5 participants did not meet the attention check criteria mentioned earlier. Their responses were excluded, leaving us with the responses of the remaining 18 participants for analysis. In total, we collected 180 question-answer pairs, distributed as follows: 48 pairs for the 3 by 3 square grid, 41 for the size 12 ring grid, 48 for the size 2 hexagon grid, and 43 for the size 3 triangle grid. We converted all the responses to lowercase and removed all English articles (a, an, the) from both the human responses and the ground truth. A response was considered "correct" only if it matched the ground truth exactly. The results can be found in Table 4.

	Square	Ring	Hexagon	Triangle	Aggregated
Human	0.90	0.78	0.41	0.58	0.67
GPT-4	0.71	0.21	0.07	0.20	0.30

Table 4: Human baseline performance compared against GPT-4. The values of the GPT-4 accuracy are taken from Figure 3.

The aggregated accuracy across all the structures is 0.67, and the accuracy for each structure is 0.90 for 3 by 3 square grid, 0.78 for size 12 ring grid, 0.41 for size 2 hexagon and 0.58 for size 3 triangle grid respectively. For GPT-4, the accuracies for each structure are from Figure 3. Although human responses are not perfect, they still outperform GPT-4 by a significant margin. It is also interesting to note that, like GPT-4, non-expert humans struggle with non-square grid shapes.

6 Related Work

Some research suggests that language models have the ability to acquire implicit world models Abdou et al. (2021); Patel & Pavlick (2022); Li et al. (2021). Spatial understanding is particularly intriguing because it might seem counterintuitive that a language model, which lacks visual or sensorimotor input, can comprehend spatial structures.

Patel & Pavlick (2022) provide evidence that GPT-3 is capable of grounding spatial and cardinal direction terms in a text-based grid world. They present contextual examples of cardinal directions (e.g., north, east, northeast) and evaluate whether the model can generalize to a different subset (e.g., south, west, southwest). Our work expands upon these findings by assessing spatial understanding that necessitates the accurate construction and retention of representations of spatial structure in more challenging tasks.

Previous studies have employed text-based navigation tasks to evaluate language models. Bubeck et al. (2023) evaluate GPT-4 across various domains, including mathematics, coding, vision, medicine, law, and psychology. In one task involving embodied interaction, they create a simple map and prompt GPT-4 to explore it interactively using actions such as left, right, up, and down. A human provides feedback during the exploration. They demonstrate that GPT-4 successfully tracks all the locations and visualizes them using a generated program. However, their study only examines a single instance of a square-grid map and does not thoroughly investigate the extent of GPT-4's spatial understanding. Another similar task is present in Whittington et al. (2020) but the goal is to test structural generalization. Srivastava et al. (2023) has a task where the agent is required to determine whether it would return to its original starting position based on a set of navigation instructions. However, this task only involves providing "yes/no" answers. In the NLP community, more complex spatial reasoning tasks have been introduced, including those involving multi-hop reasoning Shi et al. (2022) and tasks that involve understanding of textual descriptions for intricate visual scenes Mirzaee et al. (2021). In contrast, our study investigates various spatial structures, such as rings, trees, hexagons, and triangles, while also requiring the language model to remember and track object names.

A concurrent work Momennejad et al. (2023) also evaluates LLMs in terms of cognitive mapping and planning abilities. While they examine a wide array of tasks, their graph structures are limited to trees, linear paths,

and social graphs. In contrast, our work is centered on a systematic evaluation of basic spatial structures, coupled with in-depth error analysis.

7 Conclusion

In this work, we investigated whether LLMs could build representations of spatial structure implicitly from their sequential inputs. We found that LLMs are able to answer questions about spatial relationships, and tend to make errors that reflect spatial proximity. However, the details of their performance depends on the task and structure — square grids are easier than other structures, and local presentation is easier than global. Overall, our results suggest that LLMs implicitly learn to represent aspects of spatial structure, though their performance is far from perfect. These findings contribute to the growing literature on the aspects of world knowledge that LLMs implicitly acquire from their language-only training.

Limitations

In our investigation into the spatial understanding of LLM, our focus lies on the zero-shot setting. We have conducted a preliminary study to examine the impact of chain-of-thought style prompting, and we observe an increase in performance for GPT-3.5. However, beyond the 3-shot setting, the performance improvement reached a plateau. Details of these studies can be found in the Appendix, and we encourage future research to explore the effects of additional variations of chain-of-thought prompting on LLM's spatial understanding. We note that the lack of complete detail about the training of GPT-4 makes understanding the origins of its strong spatial performance somewhat challenging. Investigating how smaller models fine-tuned on spatial tasks exhibit spatial understanding would be an intriguing subject for further study.

Broader Impact Statement

As large language models continue to advance and find applications in real-world scenarios, it becomes increasingly crucial to assess the risks and unintended consequences associated with such LLM-based applications. Although our study on the spatial understanding of LLMs may not directly address the reduction of harm and bias in these models, we believe it is important to comprehend their inner workings. We hope that our work contributes to the ongoing effort of understanding and exploring the mechanisms at play within LLMs.

References

Mostafa Abdou, Artur Kulmizev, Daniel Hershcovich, Stella Frank, Ellie Pavlick, and Anders Søgaard. Can Language Models Encode Perceptual Structure Without Grounding? A Case Study in Color. In *Proceedings of the 25th Conference on Computational Natural Language Learning*, pp. 109–132, Online, November 2021. Association for Computational Linguistics. doi: 10.18653/v1/2021.conll-1.9.

Sébastien Bubeck, Varun Chandrasekaran, Ronen Eldan, Johannes Gehrke, Eric Horvitz, Ece Kamar, Peter Lee, Yin Tat Lee, Yuanzhi Li, Scott Lundberg, Harsha Nori, Hamid Palangi, Marco Tulio Ribeiro, and Yi Zhang. Sparks of Artificial General Intelligence: Early experiments with GPT-4, April 2023.

A. Coutrot, E. Manley, S. Goodroe, C. Gahnstrom, G. Filomena, D. Yesiltepe, R. C. Dalton, J. M. Wiener, C. Hölscher, M. Hornberger, and H. J. Spiers. Entropy of city street networks linked to future spatial navigation ability. *Nature*, 604(7904):104–110, April 2022. ISSN 1476-4687. doi: 10.1038/s41586-022-04486-7.

Mona M Garvert, Raymond J Dolan, and Timothy EJ Behrens. A map of abstract relational knowledge in the human hippocampal–entorhinal cortex. *eLife*, 6:e17086, April 2017. ISSN 2050-084X. doi: 10.7554/eLife.17086.

Torkel Hafting, Marianne Fyhn, Sturla Molden, May-Britt Moser, and Edvard I. Moser. Microstructure of a spatial map in the entorhinal cortex. *Nature*, 436(7052):801–806, August 2005. ISSN 1476-4687. doi: 10.1038/nature03721.

Colin Lever, Stephen Burton, Ali Jeewajee, John O'Keefe, and Neil Burgess. Boundary Vector Cells in the Subiculum of the Hippocampal Formation. *Journal of Neuroscience*, 29(31):9771–9777, August 2009. ISSN 0270-6474, 1529-2401. doi: 10.1523/JNEUROSCI.1319-09.2009.

Belinda Z. Li, Maxwell Nye, and Jacob Andreas. Implicit Representations of Meaning in Neural Language Models. In *Proceedings of the 59th Annual Meeting of the Association for Computational Linguistics and the 11th International Joint Conference on Natural Language Processing (Volume 1: Long Papers)*, pp. 1813–1827, Online, August 2021. Association for Computational Linguistics. doi: 10.18653/v1/2021.acl-long.143.

Roshanak Mirzaee, Hossein Rajaby Faghihi, Qiang Ning, and Parisa Kordjamshidi. SPARTQA: A Textual Question Answering Benchmark for Spatial Reasoning. In *Proceedings of the 2021 Conference of the North American Chapter of the Association for Computational Linguistics: Human Language Technologies*, pp. 4582–4598, Online, June 2021. Association for Computational Linguistics. doi: 10.18653/v1/2021.naacl-main.364.

Ida Momennejad, Hosein Hasanbeig, Felipe Vieira, Hiteshi Sharma, Robert Osazuwa Ness, Nebojsa Jojic, Hamid Palangi, and Jonathan Larson. Evaluating Cognitive Maps and Planning in Large Language Models with CogEval, September 2023.

J. O'Keefe and J. Dostrovsky. The hippocampus as a spatial map. Preliminary evidence from unit activity in the freely-moving rat. *Brain Research*, 34(1):171–175, November 1971. ISSN 0006-8993. doi: 10.1016/0006-8993(71)90358-1.

Roma Patel and Ellie Pavlick. Mapping Language Models to Grounded Conceptual Spaces. In *International Conference on Learning Representations*, January 2022.

Zhengxiang Shi, Qiang Zhang, and Aldo Lipani. StepGame: A New Benchmark for Robust Multi-Hop Spatial Reasoning in Texts. *Proceedings of the AAAI Conference on Artificial Intelligence*, 36(10):11321–11329, June 2022. ISSN 2374-3468. doi: 10.1609/aaai.v36i10.21383.

Aarohi Srivastava, Abhinav Rastogi, Abhishek Rao, Abu Awal Md Shoeb, Abubakar Abid, Adam Fisch, Adam R. Brown, Adam Santoro, Aditya Gupta, Adrià Garriga-Alonso, Agnieszka Kluska, Aitor Lewkowycz, Akshat Agarwal, Alethea Power, Alex Ray, Alex Warstadt, Alexander W. Kocurek, Ali Safaya, Ali Tazarv, Alice Xiang, Alicia Parrish, Allen Nie, Aman Hussain, Amanda Askell, Amanda Dsouza, Ambrose Slone, Ameet Rahane, Anantharaman S. Iyer, Anders Johan Andreassen, Andrea Madotto, Andrea Santilli, Andreas Stuhlmüller, Andrew M. Dai, Andrew La, Andrew Lampinen, Andy Zou, Angela Jiang, Angelica Chen, Anh Vuong, Animesh Gupta, Anna Gottardi, Antonio Norelli, Anu Venkatesh, Arash Gholamidavoodi, Arfa Tabassum, Arul Menezes, Arun Kirubarajan, Asher Mullokandov, Ashish Sabharwal, Austin Herrick, Avia Efrat, Aykut Erdem, Ayla Karakaş, B. Ryan Roberts, Bao Sheng Loe, Barret Zoph, Bartłomiej Bojanowski, Batuhan Özyurt, Behnam Hedayatnia, Behnam Neyshabur, Benjamin Inden, Benno Stein, Berk Ekmekci, Bill Yuchen Lin, Blake Howald, Bryan Orinion, Cameron Diao, Cameron Dour, Catherine Stinson, Cedrick Argueta, Cesar Ferri, Chandan Singh, Charles Rathkopf, Chenlin Meng, Chitta Baral, Chiyu Wu, Chris Callison-Burch, Christopher Waites, Christian Voigt, Christopher D. Manning, Christopher Potts, Cindy Ramirez, Clara E. Rivera, Clemencia Siro, Colin Raffel, Courtney Ashcraft, Cristina Garbacea, Damien Sileo, Dan Garrette, Dan Hendrycks, Dan Kilman, Dan Roth, C. Daniel Freeman, Daniel Khashabi, Daniel Levy, Daniel Moseguí González, Danielle Perszyk, Danny Hernandez, Danqi Chen, Daphne Ippolito, Dar Gilboa, David Dohan, David Drakard, David Jurgens, Debajyoti Datta, Deep Ganguli, Denis Emelin, Denis Kleyko, Deniz Yuret, Derek Chen, Derek Tam, Dieuwke Hupkes, Diganta Misra, Dilyar Buzan, Dimitri Coelho Mollo, Diyi Yang, Dong-Ho Lee, Dylan Schrader, Ekaterina Shutova, Ekin Dogus Cubuk, Elad Segal, Eleanor Hagerman, Elizabeth Barnes, Elizabeth Donoway, Ellie Pavlick, Emanuele Rodolà, Emma Lam, Eric Chu, Eric Tang, Erkut Erdem, Ernie Chang, Ethan A. Chi, Ethan Dyer, Ethan Jerzak, Ethan Kim, Eunice Engefu Manyasi, Evgenii Zheltonozhskii, Fanyue Xia, Fatemeh Siar, Fernando Martínez-Plumed, Francesca Happé, Francois Chollet, Frieda Rong, Gaurav Mishra, Genta Indra Winata, Gerard de Melo, Germán Kruszewski, Giambattista Parascandolo, Giorgio Mariani, Gloria Xinyue Wang, Gonzalo Jaimovitch-Lopez, Gregor Betz, Guy Gur-Ari, Hana Galijasevic, Hannah Kim, Hannah Rashkin, Hannaneh Hajishirzi, Harsh Mehta, Hayden

Bogar, Henry Francis Anthony Shevlin, Hinrich Schuetze, Hiromu Yakura, Hongming Zhang, Hugh Mee Wong, Ian Ng, Isaac Noble, Jaap Jumelet, Jack Geissinger, Jackson Kernion, Jacob Hilton, Jaehoon Lee, Jaime Fernández Fisac, James B. Simon, James Koppel, James Zheng, James Zou, Jan Kocon, Jana Thompson, Janelle Wingfield, Jared Kaplan, Jarema Radom, Jascha Sohl-Dickstein, Jason Phang, Jason Wei, Jason Yosinski, Jekaterina Novikova, Jelle Bosscher, Jennifer Marsh, Jeremy Kim, Jeroen Taal, Jesse Engel, Jesujoba Alabi, Jiacheng Xu, Jiaming Song, Jillian Tang, Joan Waweru, John Burden, John Miller, John U. Balis, Jonathan Batchelder, Jonathan Berant, Jörg Frohberg, Jos Rozen, Jose Hernandez-Orallo, Joseph Boudeman, Joseph Guerr, Joseph Jones, Joshua B. Tenenbaum, Joshua S. Rule, Joyce Chua, Kamil Kanclerz, Karen Livescu, Karl Krauth, Karthik Gopalakrishnan, Katerina Ignatyeva, Katja Markert, Kaustubh Dhole, Kevin Gimpel, Kevin Omondi, Kory Wallace Mathewson, Kristen Chiafullo, Ksenia Shkaruta, Kumar Shridhar, Kyle McDonell, Kyle Richardson, Laria Reynolds, Leo Gao, Li Zhang, Liam Dugan, Lianhui Qin, Lidia Contreras-Ochando, Louis-Philippe Morency, Luca Moschella, Lucas Lam, Lucy Noble, Ludwig Schmidt, Luheng He, Luis Oliveros-Colón, Luke Metz, Lütfi Kerem Senel, Maarten Bosma, Maarten Sap, Maartje Ter Hoeve, Maheen Farooqi, Manaal Faruqui, Mantas Mazeika, Marco Baturan, Marco Marelli, Marco Maru, Maria Jose Ramirez-Quintana, Marie Tolkiehn, Mario Giulianelli, Martha Lewis, Martin Potthast, Matthew L. Leavitt, Matthias Hagen, Mátyás Schubert, Medina Orduna Baitemirova, Melody Arnaud, Melvin McElrath, Michael Andrew Yee, Michael Cohen, Michael Gu, Michael Ivanitskiy, Michael Starritt, Michael Strube, Michał Swędrowski, Michele Bevilacqua, Michihiro Yasunaga, Mihir Kale, Mike Cain, Mimee Xu, Mirac Suzgun, Mitch Walker, Mo Tiwari, Mohit Bansal, Moin Aminnaseri, Mor Geva, Mozhdeh Gheini, Mukund Varma T, Nanyun Peng, Nathan Andrew Chi, Nayeon Lee, Neta Gur-Ari Krakover, Nicholas Cameron, Nicholas Roberts, Nick Doiron, Nicole Martinez, Nikita Nangia, Niklas Deckers, Niklas Muennighoff, Nitish Shirish Keskar, Niveditha S. Iyer, Noah Constant, Noah Fiedel, Nuan Wen, Oliver Zhang, Omar Agha, Omar Elbaghdadi, Omer Levy, Owain Evans, Pablo Antonio Moreno Casares, Parth Doshi, Pascale Fung, Paul Pu Liang, Paul Vicol, Pegah Alipoormolabashi, Peiyuan Liao, Percy Liang, Peter W. Chang, Peter Eckersley, Phu Mon Htut, Pinyu Hwang, Piotr Miłkowski, Piyush Patil, Pouya Pezeshkpour, Priti Oli, Qiaozhu Mei, Qing Lyu, Qinlang Chen, Rabin Banjade, Rachel Etta Rudolph, Raefer Gabriel, Rahel Habacker, Ramon Risco, Raphaël Millière, Rhythm Garg, Richard Barnes, Rif A. Saurous, Riku Arakawa, Robbe Raymaekers, Robert Frank, Rohan Sikand, Roman Novak, Roman Sitelew, Ronan Le Bras, Rosanne Liu, Rowan Jacobs, Rui Zhang, Russ Salakhutdinov, Ryan Andrew Chi, Seungjae Ryan Lee, Ryan Stovall, Ryan Teehan, Rylan Yang, Sahib Singh, Saif M. Mohammad, Sajant Anand, Sam Dillavou, Sam Shleifer, Sam Wiseman, Samuel Gruetter, Samuel R. Bowman, Samuel Stern Schoenholz, Sanghyun Han, Sanjeev Kwatra, Sarah A. Rous, Sarik Ghazarian, Sayan Ghosh, Sean Casey, Sebastian Bischoff, Sebastian Gehrmann, Sebastian Schuster, Sepideh Sadeghi, Shadi Hamdan, Sharon Zhou, Shashank Srivastava, Sherry Shi, Shikhar Singh, Shima Asaadi, Shixiang Shane Gu, Shubh Pachchigar, Shubham Toshniwal, Shyam Upadhyay, Shyamolima Shammie Debnath, Siamak Shakeri, Simon Thormeyer, Simone Melzi, Siva Reddy, Sneha Priscilla Makini, Soo-Hwan Lee, Spencer Torene, Sriharsha Hatwar, Stanislas Dehaene, Stefan Divic, Stefano Ermon, Stella Biderman, Stephanie Lin, Stephen Prasad, Steven Piantadosi, Stuart Shieber, Summer Misherghi, Svetlana Kiritchenko, Swaroop Mishra, Tal Linzen, Tal Schuster, Tao Li, Tao Yu, Tariq Ali, Tatsunori Hashimoto, Te-Lin Wu, Théo Desbordes, Theodore Rothschild, Thomas Phan, Tianle Wang, Tiberius Nkinyili, Timo Schick, Timofei Kornev, Titus Tunduny, Tobias Gerstenberg, Trenton Chang, Trishala Neeraj, Tushar Khot, Tyler Shultz, Uri Shaham, Vedant Misra, Vera Demberg, Victoria Nyamai, Vikas Raunak, Vinay Venkatesh Ramasesh, Vinay Uday Prabhu, Vishakh Padmakumar, Vivek Srikumar, William Fedus, William Saunders, William Zhang, Wout Vossen, Xiang Ren, Xiaoyu Tong, Xinran Zhao, Xinyi Wu, Xudong Shen, Yadollah Yaghoobzadeh, Yair Lakretz, Yangqiu Song, Yasaman Bahri, Yejin Choi, Yichi Yang, Yiding Hao, Yifu Chen, Yonatan Belinkov, Yu Hou, Yufang Hou, Yuntao Bai, Zachary Seid, Zhuoye Zhao, Zijian Wang, Zijie J. Wang, Zirui Wang, and Ziyi Wu. Beyond the Imitation Game: Quantifying and extrapolating the capabilities of language models. *Transactions on Machine Learning Research*, May 2023. ISSN 2835-8856.

Edward C. Tolman. Cognitive maps in rats and men. *Psychological Review*, 55:189–208, 1948. ISSN 1939-1471. doi: 10.1037/h0061626.

Hugo Touvron, Louis Martin, Kevin Stone, Peter Albert, Amjad Almahairi, Yasmine Babaei, Nikolay Bashlykov, Soumya Batra, Prajjwal Bhargava, Shruti Bhosale, Dan Bikel, Lukas Blecher, Cristian Canton Ferrer, Moya Chen, Guillem Cucurull, David Esiobu, Jude Fernandes, Jeremy Fu, Wenyin Fu, Brian Fuller,

Cynthia Gao, Vedanuj Goswami, Naman Goyal, Anthony Hartshorn, Saghar Hosseini, Rui Hou, Hakan Inan, Marcin Kardas, Viktor Kerkez, Madian Khabsa, Isabel Kloumann, Artem Korenev, Punit Singh Koura, Marie-Anne Lachaux, Thibaut Lavril, Jenya Lee, Diana Liskovich, Yinghai Lu, Yuning Mao, Xavier Martinet, Todor Mihaylov, Pushkar Mishra, Igor Molybog, Yixin Nie, Andrew Poulton, Jeremy Reizenstein, Rashi Rungta, Kalyan Saladi, Alan Schelten, Ruan Silva, Eric Michael Smith, Ranjan Subramanian, Xiaoqing Ellen Tan, Binh Tang, Ross Taylor, Adina Williams, Jian Xiang Kuan, Puxin Xu, Zheng Yan, Iliyan Zarov, Yuchen Zhang, Angela Fan, Melanie Kambadur, Sharan Narang, Aurelien Rodriguez, Robert Stojnic, Sergey Edunov, and Thomas Scialom. Llama 2: Open Foundation and Fine-Tuned Chat Models, July 2023.

James C. R. Whittington, Timothy H. Muller, Shirley Mark, Guifen Chen, Caswell Barry, Neil Burgess, and Timothy E. J. Behrens. The Tolman-Eichenbaum Machine: Unifying Space and Relational Memory through Generalization in the Hippocampal Formation. *Cell*, 183(5):1249–1263.e23, November 2020. ISSN 0092-8674. doi: 10.1016/j.cell.2020.10.024.

James C. R. Whittington, David McCaffary, Jacob J. W. Bakermans, and Timothy E. J. Behrens. How to build a cognitive map. *Nature Neuroscience*, 25(10):1257–1272, October 2022. ISSN 1546-1726. doi: 10.1038/s41593-022-01153-y.

A Prompt examples

We provide additional examples of prompts we used in Figure 12 and 13.

B Temporal distance in the global setting

For instance, in prompts for the 3 by 3 square grid structure in the global setting, such as "In the first row, we have item A, B, and C. In the second row, we have item D, E, and F, ..." the temporal distance between A and D would be 3, while the spatial distance between A and D is 1.

C Starting position bias of the square grid

In the 3 by 3 square grid, the ground truth is only present at the 1st, 3rd, 5th, and 7th nodes of the path. To qualify as a starting position bias when Temporal Distance (TD) equals 1, the ground truth would need to occur at the 2nd node of the path. Consequently, there is no contribution from the starting position bias when TD = 1.

D Chain-of-thought prompting

In the case of in-context learning experiments, we used the following system prompt: "You are given a task to solve. Make sure to output a final answer after "Answer:"." We include in-context examples in the user prompt in the following format: "Question:\n [question] \n Explanation:\n [explanation] \n Answer:\n [answer]." An example prompt is given in Figure 15.

Question: "You have been given a 3 by 3 square grid. Starting from a vertex, you will move along the edges of the grid. Initially, you are positioned at the top right corner of the grid, where you find a breastplate. You move down by one step, where you find a hummingbird. You move down by one step, where you find an eastern diamondback rattlesnake. You move left by one step, where you find a basketball. You move up by one step, where you find a pulled rickshaw. You move left by one step, where you find a Black and Tan Coonhound. You move up by one step, where you find a breakwater. You move right by one step, where you find a sea cucumber. You move right by one step. What will you find?"
Answer: "breastplate"

Question: "You have been given a 3 by 3 square grid. Starting from a vertex, you will move along the edges of the grid. Initially, you are positioned at the top left corner of the grid, where you find a cock. You move down by one step, where you find a geyser. You move right by one step, where you find a jellyfish. You move up by one step, where you find an impala. You move right by one step, where you find a box turtle. You move down by one step, where you find an espresso machine. You move down by one step, where you find a bib. You move left by one step, where you find a megalith. You move up by one step. What will you find?"
Answer: "jellyfish"

(a) 4 by 4 square grid with 8 exploration steps

Question: "You have been given an equilateral triangular tile map consisting of 3 rows, where the first row has one tile, the second row has three tiles, and so on, so that the i th row has 2*i-1 tiles. Starting from a vertex, you will move along the edges of these tiles. Initially, you are positioned at the top corner of the map, where you find an ear. You move down-left by one step, where you find a sundial. You move down-left by one step, where you find a flagpole. You move down-right by one step, where you find a West Highland White Terrier. You move right by one step, where you find a Sussex Spaniel. You move up-right by one step, where you find a howler monkey. You move left by one step, where you find a Basset Hound. You move up-right by one step, where you find an ice pop. You move up-left by one step. What will you find?"
Answer: "ear"

Question: "You have been given an equilateral triangular tile map consisting of 3 rows, where the first row has one tile, the second row has three tiles, and so on, so that the i th row has 2*i-1 tiles. Starting from a vertex, you will move along the edges of these tiles. Initially, you are positioned at the bottom right corner of the map, where you find a measuring cup. You move left by one step, where you find a binoculars. You move left by one step, where you find a rotary dial telephone. You move left by one step, where you find a space heater. You move up-right by one step, where you find a bolo tie. You move right by one step, where you find an African bush elephant. You move up-right by one step, where you find a ladle. You move left by one step, where you find an English Setter. You move down-left by one step. What will you find?"
Answer: "bolo tie"

(b) Size-3 triangular grid with 8 exploration steps

Question: "You have been given a pointy-topped regular hexagonal tile map consisting of 2 rows, where the first row has one tile and the second row has two tiles. Starting from a vertex, you will move along the edges of these tiles. Initially, you are positioned at the bottom left corner of the map, where you find a drilling rig. You move up by one step, where you find a carousel. You move up-right by one step, where you find a loupe. You move up by one step, where you find a gown. You move up-right by one step, where you find a printer. You move down-right by one step, where you find a black-footed ferret. You move down by one step, where you find a station wagon. You move down-left by one step, where you find a bath towel. You move up-left by one step. What will you find?"
Answer: "loupe"

Question: "You have been given a pointy-topped regular hexagonal tile map consisting of 2 rows, where the first row has one tile and the second row has two tiles. Starting from a vertex, you will move along the edges of these tiles. Initially, you are positioned at the top corner of the map, where you find a bucket. You move down-left by one step, where you find a gown. You move down by one step, where you find a racket. You move down-right by one step, where you find an amphibious vehicle. You move down by one step, where you find a CD player. You move down-left by one step, where you find a T-shirt. You move up-left by one step, where you find a library. You move up by one step, where you find a moped. You move up-right by one step. What will you find?"
Answer: "racket"

(c) Size-2 hexagonal grid with 8 exploration steps

Question: "You have been given a circular grid consisting of 12 connected dots. Starting from a vertex, you will move along the edges of the circular grid. Initially, you are positioned on the dot that's located at the top of the grid, where you find a milk can. You move around the ring by 4 steps in a counter-clockwise direction, where you find a mushroom. You move around the ring by 9 steps in a counter-clockwise direction, where you find a spotlight. You move around the ring by 1 step in a counter-clockwise direction, where you find a shopping basket. You move around the ring by 5 steps in a counter-clockwise direction, where you find a safety pin. You move around the ring by 8 steps in a counter-clockwise direction, where you find a poke bonnet. You move around the ring by 10 steps in a clockwise direction, where you find a Standard Schnauzer. You move around the ring by 6 steps in a counter-clockwise direction, where you find a shovel. You move around the ring by 4 steps in a clockwise direction. What will you find?"
Answer: "safety pin"

Question: "You have been given a circular grid consisting of 12 connected dots. Starting from a vertex, you will move along the edges of the circular grid. Initially, you are positioned on the dot that's located at the top of the grid, where you find a giant panda. You move around the ring by 9 steps in a clockwise direction, where you find a pickup truck. You move around the ring by 6 steps in a counter-clockwise direction, where you find a car wheel. You move around the ring by 5 steps in a clockwise direction, where you find a vulture. You move around the ring by 3 steps in a clockwise direction, where you find a quill. You move around the ring by 5 steps in a counter-clockwise direction, where you find a fountain pen. You move around the ring by 11 steps in a counter-clockwise direction, where you find a snoek. You move around the ring by 6 steps in a counter-clockwise direction, where you find a military uniform. You move around the ring by 7 steps in a clockwise direction. What will you find?"
Answer: "vulture"

(d) 12-node ring with 8 exploration steps

Figure 12: Example prompts and answers for the local setting.

Question: "You have been given a 3 by 3 square grid. In the 1st row, from left to right, we have a wok, a sleeping bag, and a balance beam. In the 2nd row, from left to right, we have a restaurant, a half-track, and a radio telescope. In the 3rd row, from left to right, we have a marimba, a Scottish Terrier, and a military uniform. You start at the position where the half-track is located, then you go left by one step, then you go up by one step, then you go right by one step, then you go right by one step, then you go down by one step, then you go down by one step, then you go left by one step, and then you go up by one step. What will you find?"
Answer: "half-track."

Figure 13: An example prompt for the global setting.

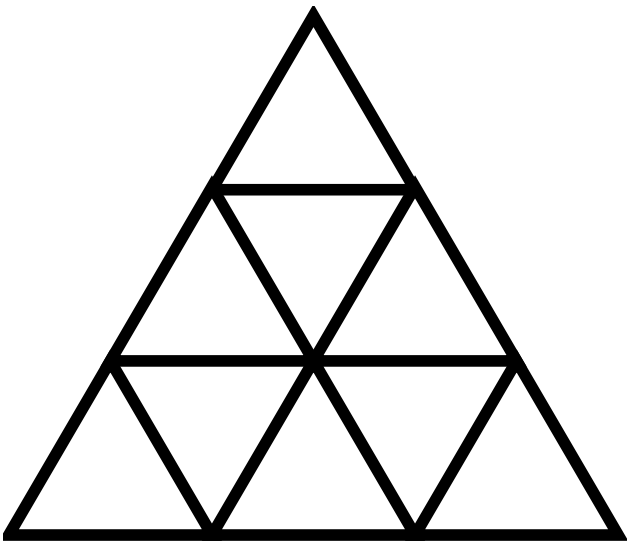

size-3 triangular grid

Figure 14: Size-3 triangular grid.

Question: "You are at the top left corner of a 2 by 2 grid, where you find box turtle. You move right by one step, where you find table lamp. You move down by one step, where you find American black bear. You move left by one step, where you find hand plane. You move up by one step. What do you find?"
Answer: "box turtle",
CoT: "We can describe our movements in the 2 by 2 grid starting from the the top left corner as follows:\n- Move right from (1,1) to (2,1)\n- Move down from (2,1) to (2,2)\n- Move left from (2,2) to (1,2)\n- Move up from (1,2) to (1,1)\nAs a result, we reach the coordinate (1,1) where we find the box turtle. Therefore, the answer is box turtle."

Figure 15: An example of Chain-of-thought style prompting for the 2 by 2 square grid.

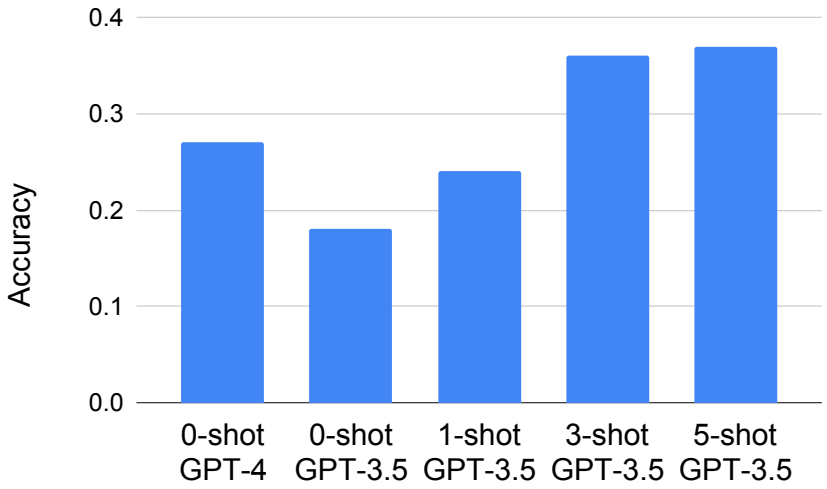

Figure 16: When chain-of-thought style prompting is employed, the accuracy of GPT-3.5 shows improvement as we increase the number of examples provided in the prompt. However, it reaches a plateau when the number of examples ranges between 3 and 5. The setting here is Ring of size 3, the number of exploration steps is 3.

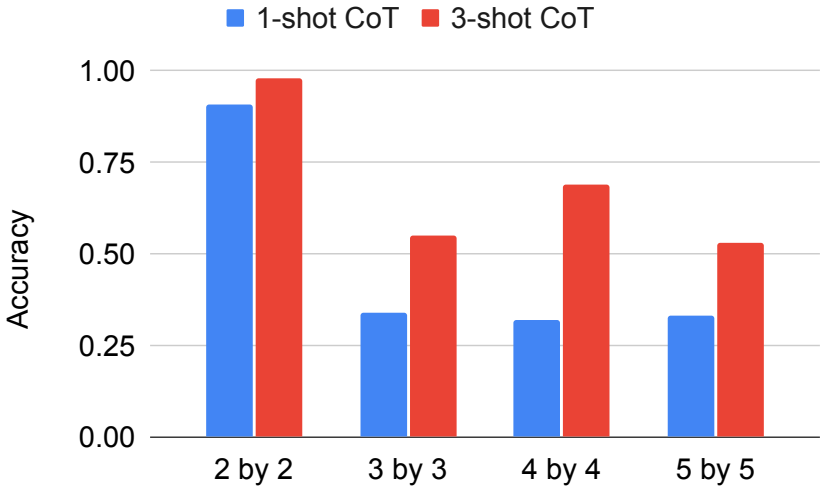

Figure 17: The accuracy for GPT-3.5 vs. the size of square structures in the global setting with exploration steps being 4. Although 3-shot CoT improves over 1-shot CoT, the performance plateaus, as we increase the size of the square structure.

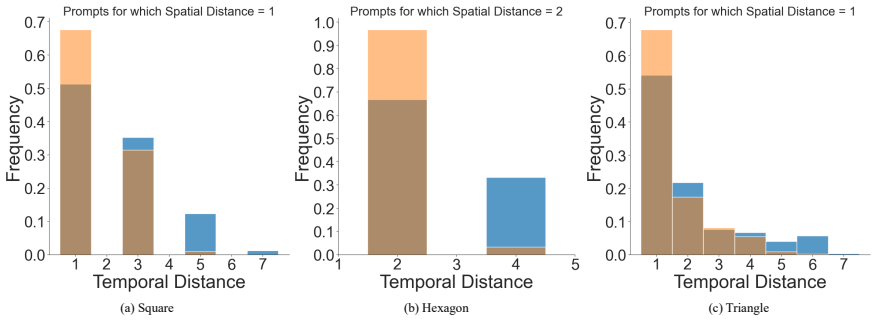

Figure 18: The temporal distance histogram conditioned on spatial distance (SD) = 1 for the square, SD = 2 for the hexagonal, and SD = 1 for the triangular grid under the local setting. These spatial distance conditions are selected because of its maximum frequency in Fig 9.